Phys Chem Minerals (2000) 27: 495–503

ORIGINAL PAPER

F. J. Gotor · M. Macías · A. Ortega · J. M. Criado

Comparative study of the kinetics of the thermal decomposition of synthetic and natural siderite samples

Received: 22 July 1999 / Accepted: 12 February 2000

Abstract The mechanism of the thermal decomposition of two siderites (a pure synthetic and a natural Mg-containing sample) has been determined from comparison of the results obtained from linear heating rate (TG) and constant rate thermal analysis (CRTA) experiments in high vacuum. The thermal decomposition of the synthetic siderite takes place approximately 200 K below the decomposition temperature of the natural sample. The mechanism and the product of the thermal decomposition are different for the siderite samples. In fact, an A_2 kinetic model describes the thermal decomposition of the synthetic siderite, whereas the thermal decomposition of the natural sample obeys an F_1 kinetic law. Decomposition products of the synthetic siderite are iron and magnetite, those of the natural siderite are wüstite and minor magnetite.

Key words Thermal decomposition · Kinetics · Siderite · CRTA

Introduction

Carbonate minerals are important constituents of many rock types. Most of the rock-forming carbonates are represented by the quaternary system $FeCO_3 - MgCO_3 - CaCO_3 - MnCO_3$ being normally characterised by complex solid solution relationships (McSwiggen 1993a, b). Natural samples of siderite ($FeCO_3$) often show a significant amount of substitution of Mg, Ca, Mn for iron in the lattice (Fisher et al. 1998; Damyanov 1998). Pure or nearly pure siderite is seldom found.

F. J. Gotor · M. Macías · A. Ortega · J. M. Criado (✉)
Instituto de Ciencia de Materiales de Sevilla
Centro Mixto Universidad de Sevilla-CSIC
Centro de Investigaciones Isla de la Cartuja,
C/Américo Vespucio SN. 41092 Sevilla, Spain
e-mail: jmcriado@cica.es
Tel.: +34-5-954489547
Fax: +34-5-954460665

The thermal decomposition of the mineral siderite is a topic of interest because of the industrial relevance of this mineral, for instance, in the processing of oil shales (Patterson 1994) or in the combustion of coals (Ram et al. 1995; Ten Brink et al. 1996). Most of the studies concern the influence of the experimental conditions, especially the atmosphere, on the nature of the final product (Gallagher and Warne 1981). This final product is generally hematite (α-Fe_2O_3) in an oxidising atmosphere, magnetite (Fe_3O_4) in a CO_2 atmosphere, and magnetite and wüstite (FeO) in an inert atmosphere or in vacuum. It has been shown in recent papers (Ding et al. 1996, 1998) that wüstite is an excellent raw material for manufacturing hard magnetic Fe/Fe_3O_4 composites with a very high coercivity. Thus, natural siderite samples would be a potential raw material for producing iron/ceramic magnets with high coercivity.

However, few efforts have been directed to establishing the kinetics of the thermal dissociation of siderite (Kubas and Szalkowicz 1971; Zakharov and Adonyi 1986; Dhupe and Gokarn 1990; Jagtap et al. 1992). Table 1 shows the kinetic data from the literature concerning the thermal decomposition of siderite. The discrepancy observed in the results reported by different authors may perhaps be due to the experimental conditions used, provided that special precautions in order to avoid heat and mass transfer phenomena do not seem to be taken. On the other hand, the method employed by Kubas and Szalkowicz (1971) to calculate the activation energy, which does not require information concerning the kinetic model, seems to be insufficiently accurate. In addition, most kinetic studies reported in Table 1 were performed by assuming a particular kinetic model. Zakharov and Adonyi (1986) have used a method developed only for *n*-order kinetic models. Dhupe and Gokarn (1990) and Jagtap et al. (1992) considered in their studies only the Avrami-Erofeev models. In previous papers (Criado and Morales 1977; Criado et al. 1978; Criado and Ortega 1984), it has been shown that the kinetic calculation from one single non-isothermal

Table 1 Summary of the results reported in literature for the thermal decomposition of siderite

Sample	Experimental conditions	Mechanism	E (kJ mol^{-1})	Reference
Mineral siderite				
$FeCO_3$ content, 72 wt%	Vacuum	Not determined	115	Kubas and Szalkowicz (1971)
$FeCO_3$ content, 87 wt%	Nitrogen flow	$f(\alpha) = (1\text{-}\alpha)^2$	238	Zakharov and Adonyi (1986)
$FeCO_3$ content, 85 wt%	Air flow	Avrami-Erofeev $n = 3$	41	Dhupe and Gokarn (1990)
$FeCO_3$ content, 85 wt%	Air flow	Avrami-Erofeev $n = 1.5$	77	Jagtap et al. (1992)

trace leads to good correlation coefficients whatever the kinetic model considered. On the other hand, it should be noted that the natural siderite samples used in these studies show a considerable amount of substitution for iron. The variations in chemical composition can affect and complicate the interpretation of the thermal analysis. For example, the type and amount of substitution strongly influence the decomposition temperature of siderite (Hurst et al. 1993), which increases proportionally to the extent of substitution of iron by magnesium, manganese and/or calcium.

Moreover, all the published papers concerning the thermal decomposition of siderite refer to natural mineral samples instead of well-characterised pure synthetic ones. This is because $FeCO_3$, like $MgCO_3$ and $ZnCO_3$, cannot be synthesised by the conventional method of flowing CO_2 through a solution of Fe(II) salts like most of the bivalent metal carbonates, but hydrothermal methods that are not easily carried out are required. The method discovered by Vidyasagar et al. (1984) for the synthesis of magnesium, zinc and iron carbonates by precipitation at normal pressure opened a way for the use of these products as raw materials. The aim of the present work is to compare the mechanism of the thermal decomposition of a natural siderite and that of a synthetic $FeCO_3$ prepared by the method of Vidyasagar et al. (1984). Every possible kinetic model describing the decomposition reaction is considered. Moreover, the role of impurities in thermal decomposition is discussed.

The validity of kinetic analysis carried out under non-isothermal conditions is often questioned because of the influence of parameters such as gradient in temperature, gas composition, sample microstructure, etc. upon the reaction kinetics. In this study, the thermal decomposition was realised under experimental conditions that allow us to minimise the influence of heat and mass transfer phenomena. This is where the CRTA technique is especially valuable, allowing us to lower these gradients by an appropriate control of the reaction rate so that the influence of experimental conditions upon the reaction under study may be satisfactorily prevented. In previous papers (Criado et al. 1980a; Criado and Ortega 1992; Koga and Criado 1998), it has been shown that kinetic data corresponding to the thermal decomposition of $CaCO_3$ were quite independent of both the sources of the sample and the particle size, provided that transport phenomena were reduced. The use of the CRTA method for the synthesis of materials with controlled texture and structure has been recently reported in the literature (Chopra et al. 1999; Perez-Maqueda et al. 1999a, b).

Experimental

Materials and methods

A natural siderite sample from Cala (Spain) was used. Its chemical analysis by X-ray fluorescence spectrometry is:

Fe_2O_3, 44.6%; MgO, 10.8%; Mn_2O_3, 3.7%; CaO, 1.1%; SiO_2, 4.9%; others, 0.9%; ignition loss, 34.0%.

The synthetic siderite sample was obtained by the method described by Vidyasagar et al. (1984) from $FeSO_4 \cdot 7H_2O$ and $NaHCO_3$ reagents (Merck). The iron carbonate content of the synthetic siderite was 99%. The total weight loss of this sample (37.25%) agrees with the value expected for the thermal decomposition of iron carbonate (37.98%).

The X-ray powder-diffraction patterns were collected with a Siemens D501 instrument equipped with a scintillation counter using Cu K_α radiation and a graphite monochromator. The scanning rate of the goniometer was 1.2° min^{-1} for phase identification and 0.3° min^{-1} for unit cell parameter refinement. The full width at half maximum (FWHM) and the position of peaks were calculated using the software package of the diffractometer. The lattice parameters (a,c) were determined by a least-squares refinement (LSUCREB method) on the gathered XRD data (Appleman and Evans 1973).

A Cahn electrobalance connected to a conventional high vacuum system equipped with a Penning gauge was used for performing linear heating rate (TG) and constant rate thermal analysis (CRTA) experiments. The pressure of the gases generated in the reaction was continuously monitored during the TG runs. The starting sample weight of siderite (approximately 14 mg) was chosen in such a way that the pressure never exceeded the value of 10^{-4} mbar. It would be expected that under these experimental conditions the maximum decomposition rate would be small enough to avoid the influence of heat and mass transfer phenomena on the forward reaction.

The temperature control in CRTA experiments is carried out in such a way that the decomposition rate is kept constant throughout the process at a previously selected value. This was attained by interfacing the analogical output of the Penning gauge to the furnace controller in order to maintain the residual pressure in the close vicinity of the sample at a constant previously selected value. Thus, the reaction rate will be constant, provided that the pumping rate has been properly selected by means of a vacuum valve. A residual pressure of 7.5×10^{-5} mbar and a sample weight of 25 mg were used in the CRTA experiments for both the synthetic and natural siderite samples.

Kinetic analysis

Linear heating rate (TG)

Kinetic analysis of non-isothermal data recorded under constant heating rate was carried out using the Coats and Redfern (1964) method:

$$\ln g(\alpha) - 2\ln T \cong \ln\frac{AR}{E\beta} - \frac{E}{RT} \quad , \tag{1}$$

where α is the reacted fraction at time t, β is the heating rate, E is the activation energy, A is the preexponential factor, T is the absolute temperature, and $g(\alpha)$ is a function depending on the reaction mechanism (Table 2).

The plot of the left-hand side of Eq. (1) as a function of the reciprocal of the temperature gives a straight line whose slope yields the activation energy with an error less than 4%, provided that E/RT is greater than 5 (Criado and Ortega 1985). However, Criado and Ortega (1984) have shown that any $g(\alpha)$ function (Table 2) fulfils Eq. (1). Therefore, the kinetic model followed by a solid-state reaction cannot be identified from the analysis of a single TG trace (Criado et al. 1990). As an example, Fig. 1 shows two TG curves simulated by numerical methods with a precision better than 10^{-5}%, assuming the following parameters:

curve 1: F_1 model, $E = 150$ kJ mol^{-1}, $A = 2 \times 10^6$ s^{-1}, $\beta = 5$ K min^{-1},
curve 2: A_3 model, $E = 41$ kJ mol^{-1}, $A = 0.2$ s^{-1}, $\beta = 5$ K min^{-1}.

The two curves coincide over the entire α-reacted fraction range despite they were calculated by assuming different kinetic models and different kinetic parameters.

Constant rate thermal analysis (CRTA)

The CRTA data (recorded at a constant decomposition rate, C) were analysed by means of the following equation (Criado 1979):

$$\ln\frac{1}{f(\alpha)} = \ln\frac{A}{C} - \frac{E}{RT} \quad , \tag{2}$$

where $f(\alpha)$ is also a function depending on the reaction mechanism. Therefore, the kinetic parameters of the reaction can be obtained from the plot of the left-hand side of Eq. (2) against the reciprocal of the temperature. It should be remarked that in the case of processes described by a $f(\alpha) = (1-\alpha)^n$ function (i.e., R_2, R_3 and F_1 models), Eq. (2) becomes:

$$\ln\frac{1}{1-\alpha} = \ln\frac{A}{nC} - \frac{E}{nRT} \quad . \tag{3}$$

Equation (3) points out that it is not possible to determine simultaneously n and E from a single CRTA trace.

In previous papers (Criado et al. 1980a, b), it has been reported that CRTA allows a better discrimination of the actual kinetic model fitted by a solid-state reaction than conventional TG. This is demonstrated in Fig. 2, which shows two CRTA theoretical curves calculated from Eq. (2) by assuming the same kinetic parameters used for calculating the corresponding TG curves in Fig. 1 (a C

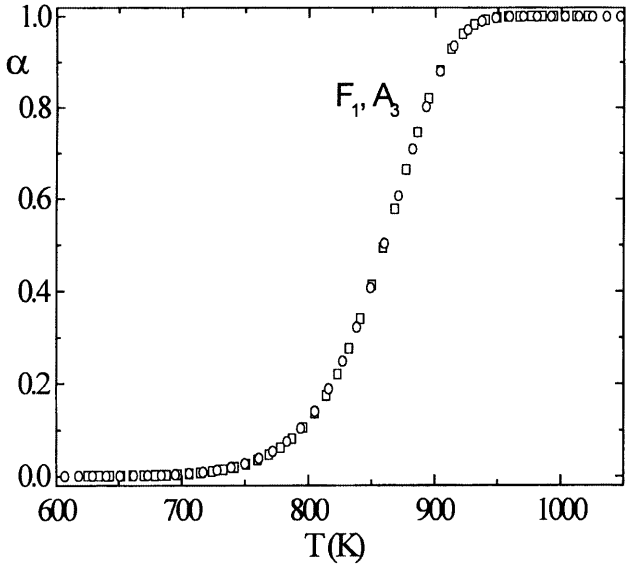

Fig. 1 Two identical TG curves calculated by assuming a linear heating rate $\beta = 5$ K min^{-1} and two different kinetic models and different kinetic parameters: *curve 1* (□) F_1 model, $E = 150$ kJ mol^{-1}, $A = 2 \times 10^6$ s^{-1}; *curve 2* (○): A_3 model, $E = 41$ kJ mol^{-1}, $A = 0.2$ s^{-1}

Table 2 Algebraic expressions for the $f(\alpha)$ and $g(\alpha)$ functions for the most common mechanisms in solid-state reactions

Mechanism	Symbol[a]	$f(\alpha)$	$g(\alpha)$
Phase boundary controlled reaction (contracting area – bidimensional shape)	R_2	$(1-\alpha)^{1/2}$	$2[1-(1-\alpha)^{1/2}]$
Phase boundary controlled reaction (contracting volume – tridimensional shape)	R_3	$(1-\alpha)^{2/3}$	$3[1-(1-\alpha)^{1/3}]$
Unimolecular decay law (instantaneous nucleation and unidimensional growth)	F_1[b]	$(1-\alpha)$	$-\ln(1-\alpha)$
Random nucleation and growth of nuclei (Avrami–Erofeev equation)	An	$n(1-\alpha)[-\ln(1-\alpha)]^{1-1/n}$	$[-\ln(1-\alpha)]^{1/n}$
One-dimensional diffusion (parabolic law)	D_1	$1/2\alpha$	α^2
Two-dimensional diffusion (bidimensional particle shape)	D_2	$1/[-\ln(1-\alpha)]$	$(1-\alpha)\ln(1-\alpha) + \alpha$
Three-dimensional diffusion (tridimensional particle shape) Jander equation	D_3	$3(1-\alpha)^{2/3}/2[(1-\alpha)^{1/3}]$	$\left[1-(1-\alpha)^{1/3}\right]^2$
Three-dimensional diffusion (tridimensional particle shape) Ginstein–Brounshtein equation	D_4	$3/2[(1-\alpha)^{-1/3}-1]$	$(1-2\alpha/3)-(1-\alpha)^{2/3}$

[a] The symbols proposed by Sharp et al. (1966) have been used
[b] This kinetic model can be identified with an Avrami-Erofeev kinetic equation with $n = 1$

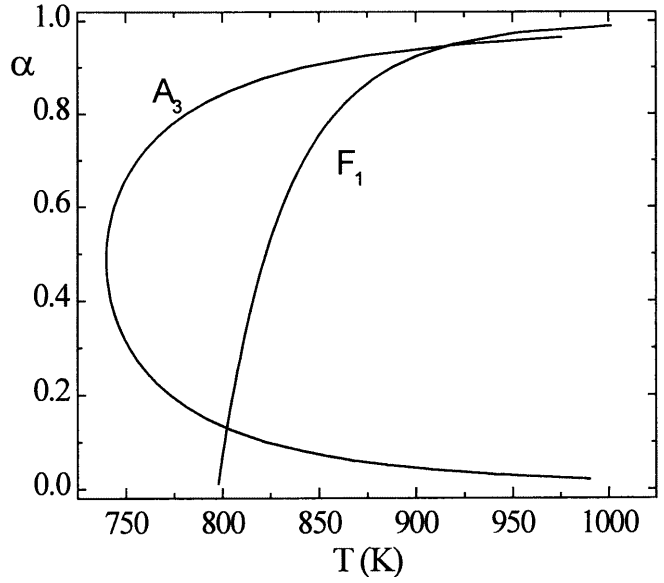

Fig. 2 Discrimination between both kinetic models of Fig. 1 by CRTA; C = 3×10^{-4} s^{-1}: *curve 1* F_1 model, E = 150 kJ mol^{-1}, A = 2×10^6 s^{-1}; *curve 2* A_3 model, E = 41 kJ mol^{-1}, A = 0.2 s^{-1}

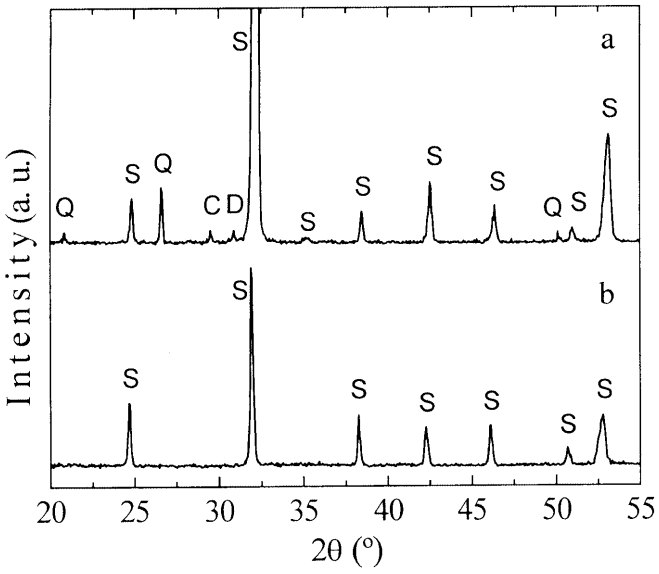

Fig. 3a, b X-ray diffraction patterns of **a** the natural siderite from Cala (Spain) and **b** the pure synthetic siderite: *S* siderite; *C* calcite; *D* dolomite; *Q* quartz

value of 3×10^{-4} s^{-1} was used in the calculation). In this case, both models (F_1 and A_3) are clearly distinguishable. Moreover, it has been shown (Criado 1979; Gotor et al. 1998) that the same kinetic parameters are obtained from the kinetic analysis of TG and CRTA traces only if the kinetic law really fitted by the reaction has been selected for performing the calculations. The heating rate, β, of the TG curve and the constant decomposition rate, C, of the CRTA trace must be selected in such a way that the overall reaction takes place at approximately the same range of temperatures. This precaution in the two TG and CRTA experiments to be compared is of interest provided that the mechanism of solid-state reactions can be strongly dependent upon temperature. In summary, a comparison of the results obtained independently from the kinetic analysis of TG and CRTA experiments would be a valuable tool for discerning the mechanism of the thermal decomposition of siderite.

Results and discussion

Figure 3a shows the X-ray diffraction pattern of the natural siderite. Minor amounts of calcite, dolomite and quartz are present. Figure 3b shows the X-ray diffraction pattern of the synthetic $FeCO_3$ sample. A comparison of both XRD patterns points out that the diffraction peaks of the natural siderite are shifted to higher angles. This fact reflects an expanded unit cell probably due to the substitution of Fe^{2+} by Mg^{2+}, the major impurity. The unit cell parameters of the natural siderite refined from the XRD pattern are a = 4.6739(5) and c = 15.246(2). These parameters are consistent with a nominal composition of $\sim (Fe_{0.7}Mg_{0.3})CO_3$ according to the results recently reported by Chai and Navrotsky (1996), where they show a linear relationship (Vegard's law) of the unit cell parameters with the composition in the $FeCO_3$–$MgCO_3$ solid solution. This result is in agreement with the chemical analysis by X-ray fluorescence and then the natural siderite can be considered as an Mg siderite with a high Mg content (~30 mol%). Unit cell parameters of the synthetic siderite [a = 4.6919(8) and c = 15.407(2)] coincide well with those of the JCPDF file 29-696 corresponding to the iron carbonate [a = 4.6935(2) and c = 15.386(8)]. On the other hand, the diffraction peak widths (FWHM) of two siderites are almost the same (0.215° and 0.200° for the natural and synthetic siderites, respectively), and close to the instrumental broadening (0.170°), which suggests very good crystallinity for both samples.

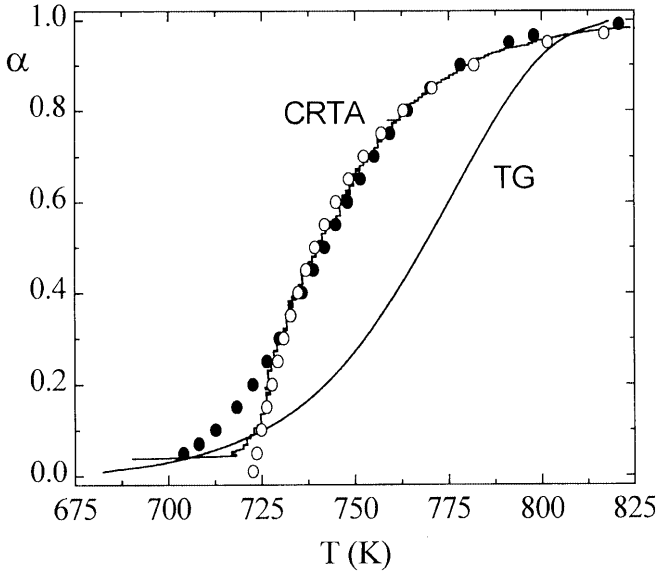

Fig. 4 TG curve obtained at a heating rate of 0.52 K min^{-1} and CRTA curve obtained at a decomposition rate of 2.45×10^{-3} min^{-1} for the natural siderite. Theoretical CRTA curve calculated from the kinetic parameters reported in Table 3 corresponding to the F_1 (○) and $A_{0.5}$ (●) kinetic laws

Figure 4 shows the TG recorded at a heating rate $\beta = 0.52$ K min^{-1} together with the corresponding CRTA curve obtained by selecting a constant decomposition rate C = 2.45×10^{-3} min^{-1} for the natural siderite. On the other hand, the synthetic siderite TG curve obtained at a heating rate $\beta = 0.52$ K min^{-1} is compared in Fig. 5 with the corresponding CRTA curve recorded at a constant decomposition rate C = 3.52×10^{-3} min^{-1}. Two interesting features can be observed by comparing Figs. 4 and 5. Firstly, natural siderite decomposes at a temperature approximately 200 K higher than the corresponding one to synthetic $FeCO_3$. This behaviour can be associated with the high substitution content present in the natural siderite studied in this work. It has been already shown (Patterson et al. 1991) that increasing magnesium, manganese or calcium content increases the temperature of the siderite decomposition. The second interesting feature is related with the shape of CRTA traces. The different shape implies a different mechanism for the thermal decomposition of both samples (Criado et al. 1990). Thus, the natural siderite seems to obey an *n*-order kinetic model (CRTA trace is concave with regards to the temperature axis) and the synthetic one could be described by an Avrami-Erofeev law (α versus T CRTA plot shows a minimum).

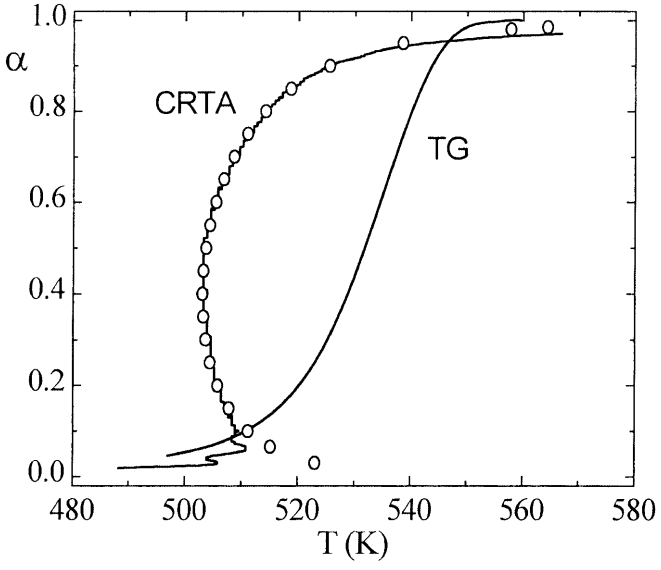

Fig. 5 TG curve obtained at a heating rate of 0.52 K min^{-1} and CRTA curve obtained at a decomposition rate of 3.52×10^{-3} min^{-1} for the synthetic siderite. (○) Theoretical CRTA curve calculated from the kinetic parameters reported in Table 4 for the A_2 kinetic model

The kinetic parameters of the thermal decomposition of the natural siderite obtained from the kinetic analysis of the TG and CRTA curves in Fig. 4 by using Eqs. (1) and (2) [after substituting the different g(α) or f(α) functions included in Table 2] are shown in Table 3. The kinetic parameters, E and A, determined from TG and CRTA curves, show a reasonable agreement (192 and 182 kJ mol^{-1}, and 21.65 and 20.22 for E and ln A, respectively) only if it is assumed that the reaction fits the F_1 kinetic model. Figure 4 also shows that the theoretical CRTA curve calculated from the kinetic parameters corresponding to the F_1 kinetic model, reported in Table 3, matches the experimental curve quite well. It could be argued that both reasonably good correlation coefficients and an agreement between the activation energies obtained from TG and CRTA experiments (397 and 372 kJ mol^{-1}, respectively) better than 7% could be also achieved by assuming an $A_{0.5}$ kinetic model (Table 3). However, the theoretical curve calculated from the kinetic parameters obtained for this model does not sufficiently agree with the experimental one, as shown in Fig. 4. In addition, the characteristic inflexion point of the $A_{0.5}$ kinetic model is not observed in the experimental CRTA trace. Moreover, the plot of the experimental CRTA data (Fig. 6) according to Eq. (2) after substituting the f(α) function corresponding to F_1 and $A_{0.5}$ kinetic models points out that a strong deviation from the straight line takes place for α values lower than 0.43 if the $A_{0.5}$ kinetic model is assumed. Therefore, it can be concluded that the thermal decomposition reaction of the natural siderite obeys an F_1 kinetic model.

Table 4 reports the results obtained from the kinetic analysis of the TG and CRTA curves shown in Fig. 5 using the same procedure previously described for the calculation of the data included in Table 3. It can be observed that the best agreement between the kinetic parameters obtained from CRTA and TG experiments is achieved by assuming that the thermal decomposition of

Table 3 Kinetic parameters calculated from TG and CRTA curves of Fig. 4 for the thermal decomposition of the natural siderite

Mechanism	TG ($\beta = 0.52$ K min^{-1})			CRTA (C = 2.45×10^{-3} min^{-1})		
	E (kJ mol^{-1})	ln A (s^{-1})	r	E (kJ mol^{-1})	ln A (s^{-1})	r
R_2	160 ± 1	16.30 ± 0.03	0.9988	91 ± 1	5.06 ± 0.02	0.9971
R_3	170 ± 1	18.00 ± 0.02	0.9994	121 ± 1	10.11 ± 0.03	0.9971
F_1[a]	**192 ± 1**	**21.65 ± 0.01**	**0.9999**	**182 ± 1**	**20.22 ± 0.04**	**0.9971**
$A_{0.5}$	397 ± 1	54.07 ± 0.01	0.9999	372 ± 1	51.24 ± 0.16	0.9906
A_2	90 ± 1	5.04 ± 0.01	0.9999	87 ± 1	4.36 ± 0.12	0.9086
A_3	56 ± 1	−0.72 ± 0.01	0.9999	56 ± 1	−1.10 ± 0.15	0.7451
A_4	38 ± 1	−3.73 ± 0.01	0.9999	40 ± 1	−3.92 ± 0.17	0.5884
D_2	312 ± 1	39.41 ± 0.08	0.9979	190 ± 1	20.22 ± 0.18	0.9546
D_3	353 ± 1	44.70 ± 0.05	0.9995	283 ± 1	34.24 ± 0.17	0.9820
D_4	326 ± 1	40.15 ± 0.07	0.9986	223 ± 1	24.13 ± 0.18	0.9685

[a] In bold, best agreement between TG and CRTA kinetic analysis

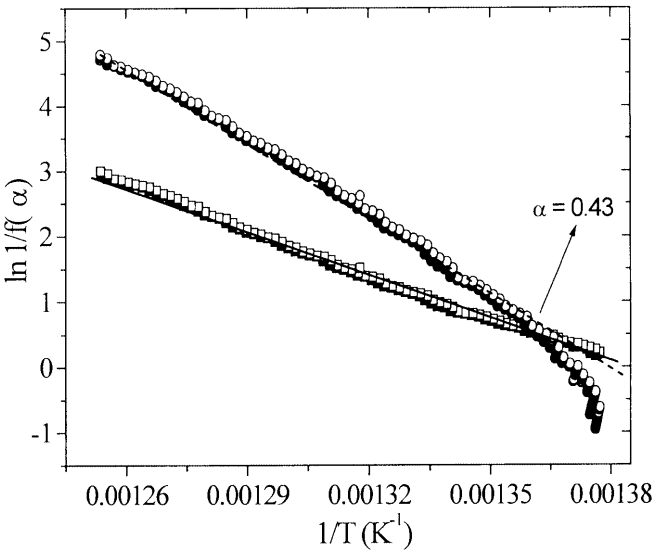

Fig. 6 Plots of the left-hand side of Eq. (2) as a function of the inverse of the temperature calculated from the CRTA data of Fig. 4 after assuming the f(α) function corresponding to the F_1 (□) and $A_{0.5}$ (○) kinetic models, respectively

the synthetic siderite follows an A_2 kinetic model. Only the theoretical CRTA curve (also shown in Fig. 5) calculated by assuming the kinetic parameters reported in Table 4 for the A_2 kinetic model fits the experimental data quite well.

F_1 and A_2 kinetic equations belong to the Avrami-Erofeev kinetic models with a coefficient $n = 1$ and $n = 2$, respectively. The value of this parameter depends on the mechanism of formation of nuclei and the number of spatial dimensions in which they grow, as summarised in Table 5. This table shows that a same n-parameter would describe different reaction mechanisms. However, taking into account that both synthetic and natural siderite partially substituted with Mg^{2+} have a calcite-type crystalline structure, it would be reasonable to assume a similar behaviour for the thermal decomposition of these two samples. The results here obtained would be interpreted by considering that the reaction mechanism implies the formation of nuclei and their subsequent growth through a diffusion process. Such a mechanism leads to the fitting of the kinetic data to an Avrami-Erofeev kinetic model with a coefficient $n = 2$, as here reported for the thermal decomposition of the synthetic $FeCO_3$. Moreover, it is worth noting that, generally, the nucleation rate increases very quickly on increasing the reaction temperature, and an instantaneous nucleation could be favoured if the reaction temperature were large enough. It has previously been shown that the thermal decomposition of natural siderite starts at considerably higher temperature than the synthetic one because of the

Table 4 Kinetic parameters calculated from TG and CRTA curves of Fig. 5 for the thermal decomposition of synthetic $FeCO_3$

Mechanism	TG (β = 0.52 K min^{-1})			CRTA (C = 3.52 × 10^{-3} min^{-1})		
	E (kJ mol^{-1})	ln A (s^{-1})	r	E (kJ mol^{-1})	ln A (s^{-1})	r
R_2	185 ± 1	34.05 ± 0.09	0.9981	99 ± 3	14.10 ± 0.60	0.8253
R_3	196 ± 1	36.69 ± 0.08	0.9986	132 ± 3	22.04 ± 0.80	0.8253
F_1	220 ± 1	42.35 ± 0.08	0.9988	198 ± 5	37.93 ± 1.20	0.8253
$A_{0.5}$	450 ± 1	94.52 ± 0.17	0.9988	390 ± 15	83.69 ± 3.65	0.6885
A_2[a]	**106 ± 1**	**15.88 ± 0.04**	**0.9987**	**102 ± 1**	**14.71 ± 0.08**	**0.9957**
A_3	68 ± 1	6.86 ± 0.03	0.9986	70 ± 2	6.80 ± 0.44	0.8146
A_4	48 ± 1	2.24 ± 0.02	0.9984	54 ± 3	2.75 ± 0.64	0.5958
D_2	356 ± 1	72.01 ± 0.19	0.9975	192 ± 10	35.32 ± 2.45	0.5718
D_3	402 ± 1	81.12 ± 0.16	0.9986	293 ± 13	58.18 ± 3.05	0.6487
D_4	371 ± 1	74.02 ± 0.18	0.9980	227 ± 11	42.28 ± 2.65	0.6052

[a] In bold, best agreement between TG and CRTA kinetic analysis

Table 5 Physical meaning of the Avrami-Erofeev kinetic coefficient

Type of nucleation and geometry of growing	Law of growing of nuclei	
	Chemical reaction (linear law)	Diffusion law (parabolic law)
	n	*n*
Instantaneous nucleation and one-dimensional growth	1.0	0.5
Instantaneous nucleation and two-dimensional growth	2.0	1.0
Instantaneous nucleation and three-dimensional growth	3.0	1.5
Constant rate of nucleation and one-dimensional growth	2.0	1.5
Constant rate of nucleation and two-dimensional growth	3.0	2.0
Constant rate of nucleation and three-dimensional growth	4.0	2.5

stabilisation of the structure produced by the magnesium substitution, which explains the higher activation energy for the thermal decomposition of the substituted sample. Thus, it could occur that the nucleation becomes instantaneous in the natural sample and growth of the nuclei continues to take place by a two-dimensional diffusion-controlled process, which would explain that the kinetic data fit an F_1 kinetic model. The two-dimensional controlled rate could perhaps be understood by considering the calcite structure of the above compounds. It has been shown (Criado and Trillo 1975) that the calcite structure, if oriented on plane (1 1 1), can consist of distorted cubic packing of cations, with CO_3^{2-} ions occupying all the octahedral interstices contained between successive plains ABCABC... of cations. If we bear in mind that the cations have a larger mobility than the anions, it could be proposed that the decomposition rate of siderite is controlled by the cation diffusion on this plane. The calcite/aragonite phase transition induced by mechanical grinding of $CaCO_3$ was also explained by considering the ionic mobility on the (1 1 1) plane (Criado and Trillo 1975).

The composition of the final products yielded from the thermal decomposition of siderite is another important point to be considered. Figure 7 shows the X-ray diffraction patterns of the final products of the thermal decomposition of natural and synthetic siderites obtained after recording the TG diagrams included in Figs. 4 and 5, respectively. The data included in Fig. 7a indicate that FeO (wüstite) mainly constitutes the decomposition product of the natural siderite. This phase must be considered as a magnesium iron oxide ($Mg_{1-x}Fe_xO$, JCPDF file 35-1393) rather than a pure FeO phase. Figure 8 compares the XRD pattern of the wüstite phase yielded from the natural siderite and the

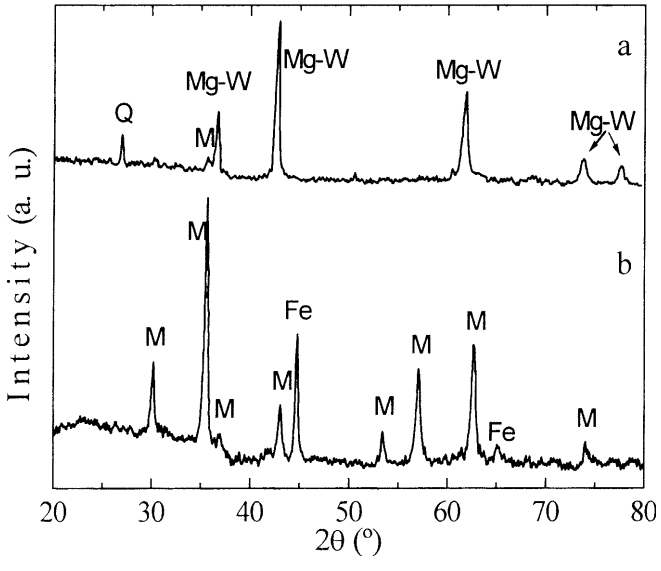

Fig. 7a, b X-ray diffraction patterns of the products of the thermal decomposition of **a** the natural siderite and **b** the synthetic siderite: *Mg-W* Mg-substituted wüstite; *M* magnetite; *Q* quartz; *Fe* iron

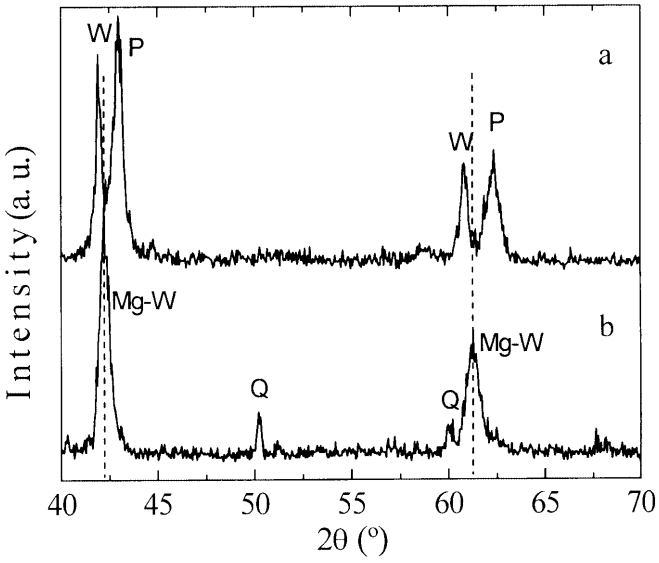

Fig. 8a, b X-ray diffraction patterns of **a** a mixture of pure FeO (*W*) and MgO (*P*) (70/30 mol%). **b** The product of the thermal decomposition of the natural siderite: *Mg-W* Mg-substituted siderite; *Q* quartz

XRD pattern of a mixture of pure FeO and MgO with a composition of 70 and 30 mol% for FeO and MgO, respectively. This figure reflects a shift in the XRD peaks of the wüstite phase yielded from the natural siderite to higher angles with respect to the pure FeO phase. This behaviour is similar to that observed in the natural siderite. XRD peaks of MgO are not observed. Therefore, Mg^{2+} impurities of the natural siderite must dissolve in the wüstite phase during its thermal decomposition. The small amount of magnetite (Fe_3O_4) found in the final product of the thermal decomposition of this sample could be associated with the oxidation of the FeO by the carbon dioxide produced in the reaction. Carbon dioxide could be partially chemisorbed on the oxide surface during the decomposition of the carbonate, in spite of being used at high vacuum.

On the other hand, iron and magnetite constitute the product of the decomposition of the synthetic $FeCO_3$ (Fig. 7b). If we assume that the decomposition product of the synthetic siderite is also wüstite, the presence of iron and magnetite can only be explained on the basis of the equilibrium of dismutation of FeO according to the following reaction:

$$4FeO \rightarrow Fe_3O_4 + \alpha - Fe \ . \qquad (4)$$

It can be estimated from thermodynamic data of the species involved in the reaction that the forward reaction is favoured below 563 °C. Ding et al. (1998) recorded in a recent paper the DSC curve of an FeO sample. They observed an endothermic peak, corresponding to the decomposition of wüstite into Fe and Fe_3O_4 that appeared at 250 °C, followed by an exothermic peak at 560 °C corresponding to the reformation of FeO. The thermal decomposition of the synthetic siderite takes place in a range of temperatures at which the forward

reaction (4) is thermodynamically favoured. Thus, the iron and magnetite phases formed through this secondary reaction are stabilised.

Conclusions

Thermal stability of siderite is strongly affected by the partial substitution of Fe^{2+} in the cationic sublattice. We have shown that a pure synthetic siderite decomposes 200 K below the temperature of decomposition of a natural siderite with a high Mg content (30 mol%). Both the kinetics and products yielded from the thermal decomposition of the two siderite samples here studied are different. This behaviour is related to the thermal stability of each sample. The thermal decomposition of both samples takes place through the formation of wüstite, but it decomposes into iron and magnetite at the temperature range at which the thermal decomposition of the synthetic siderite occurs. The thermal decomposition of the natural siderite is completed at higher temperatures than those required for favouring the dismutation of wüstite leading to the stabilisation of this phase.

References

Appleman DE, Evans HT (1973) Least-squares and indexing software for XRD data. Document No PB-216188, US Geological Survey, Computer Contribution No 20, US National Technical Information Service, Washington, DC

Chai L, Navrotsky A (1996) Synthesis, characterization, and enthalpy of mixing of the (Fe,Mg)CO_3 solid solution. Geochim Cosmochim Acta 60: 4377–4383

Chopra GS, Real C, Alcala MD, Perez-Maqueda LA, Subrt J, Criado JM (1999) Factors influencing the texture and stability of maghemite obtained from the thermal decomposition of lepidocrocite. Chem Mater 11: 1128–1137

Coats AW, Redfern JP (1964) Kinetic parameters from thermogravimetric data. Nature 201: 68–69

Criado JM (1979) On the kinetic analysis of thermoanalytical diagrams obtained with the ''quasi-isothermal'' heating technique. Thermochim Acta 28: 307–312

Criado JM, Morales J (1977) Thermal decomposition of solids controlled by diffusion and phase-boundary processes: possible misinterpretation of the mechanism from thermogravimetric data. Thermochim Acta 19: 305–317

Criado JM, Ortega A (1984) Remarks on the discrimination of the kinetics of solid-state reactions from a single non-isothermal trace. J Therm Anal 29: 1225–1236

Criado JM, Ortega A (1985) The accuracy of equation approximating the integral of the Arrhenius equation to perform the kinetic analysis of solid state reactions. Int J Chem Kinet 17: 1365–1373

Criado JM, Ortega A (1992) A study of the influence of particle size on the thermal decomposition of $CaCO_3$ by means of constant rate thermal analysis. Thermochim Acta 195: 163–167

Criado JM, Trillo JM (1975) Effects of mechanical grinding on the texture and structure of calcium carbonate. J Chem Soc Faraday T 71: 961–966

Criado JM, Morales J, Rives V (1978) Computer kinetic analysis of simultaneously obtained TG and DTG curves. J Therm Anal 14: 221–228

Criado JM, Rouquerol F, Rouquerol J (1980a) Study of the thermal decomposition reactions in solids: comparison of the constant decomposition rate thermal analysis with the conventional TG method. Thermochim Acta 38: 109–115

Criado JM, Rouquerol F, Rouquerol J (1980b) Study of the thermal decomposition reaction mechanism of alkaline-earth carbonates under high vacuum by both thermogravimetric analysis and constant decomposition rate thermal analysis techniques. Thermochim Acta 38: 117–123

Criado JM, Ortega A, Gotor F (1990) Correlation between the shape of controlled-rate thermal analysis curves and the kinetics of solid-state reactions. Thermochim Acta 157: 171–179

Damyanov ZK (1998) Ore petrology, whole-rock chemistry and zoning of the Kremikovtsi carbonate-hosted sedimentary exhalative iron(+Mn)-barite-sulfide deposit, Western Balkan, Bulgaria. Neues Jahrb Mineral Abh 174: 1–42

Dhupe AP, Gokarn AN (1990) Studies in the thermal decomposition of natural siderites in the presence of air. Int J Miner Process 20: 209–220

Ding J, Miao WF, Street R, McCormick PG (1996) Fe_3O_4/Fe magnetic composite synthesized by mechanical alloying. Scripta Mater 35: 1307–1310

Ding J, Miao WF, Piraults E, Street R, McCormick PG (1998) Structural evolution of Fe + Fe_2O_3 during mechanical milling. J Magn Magn Mater 177–181: 933–934

Fisher QJ, Raiswell R, Marshall JD (1998) Siderite concretions from nonmarine shales (Westphalian A) of the Pennines, England: controls on their growth and composition. J Sediment Res 68: 1034–1045

Gallagher PK, Warne SStJ (1981) Thermomagnetometry and thermal decomposition of siderite. Thermochim Acta 43: 253–267

Gotor FJ, Macías M, Ortega A, Criado JM (1998) Simultaneous use of isothermal, nonisothermal and constant rate thermal analysis (CRTA) for discerning the kinetics of the thermal dissociation of smithsonite. Int J Chem Kinet 30: 647–655

Hurst HJ, Levy JH, Patterson JH (1993) Siderite decomposition in retorting atmospheres. Fuel 72: 885–890

Jagtap SB, Pande AR, Gokarn AN (1992) Kinetics of thermal decomposition of siderite: effect of particle size. Int J Miner Process 36: 113–124

Koga N, Criado JM (1998) The influence of mass transfer phenomena on the kinetic analysis for the thermal decomposition of calcium carbonate by constant rate thermal analysis. Int J Chem Kinet 30: 737–744

Kubas Z, Szalkowicz M (1971) Application of simultaneous differential thermal analysis, thermogravimetry and analysis of the evolved gases to studies on kinetics and mechanism of complex reactions. In: Thermal analysis, vol. 2. Proc 3rd ICTA, Davos. Birkhäuser, Basel, pp 447–461

McSwiggen PL (1993a) Alternative solution model for the ternary carbonate system $CaCO_3$-$MgCO_3$-$FeCO_3$; Part I. A ternary Bragg–Willians ordering model. Phys Chem Miner 20: 33–41

McSwiggen PL (1993b) Alternative solution model for the ternary carbonate system $CaCO_3$-$MgCO_3$-$FeCO_3$; Part II. Calibration of a combined ordering model and mixing model. Phys Chem Miner 20: 42–55

Patterson JH (1994) A review of the effects of minerals in processing of Australian oil shales. Fuel 73: 321–327

Patterson JH, Hurst HJ, Levy JH (1991) Relevance of carbonate minerals in the processing of Australian Tertiary oil shales. Fuel 70: 1252–1259

Perez-Maqueda LA, Criado JM, Subrt J, Real C (1999a) Synthesis of acicular hematite catalysts with tailored porosity. Cat Lett 60: 151–156

Perez-Maqueda LA, Criado JM, Real C, Subrt J, Bohacek J (1999b) The use of constant rate thermal analysis (CRTA) for controlling the texture of hematite obtained from the thermal decomposition of goethite. J Mater Chem 9: 1839–1845

Ram LC, Tripathi PSM, Mishra SP (1995) Mössbauer spectroscopic studies on the transformations of iron-bearing minerals

during combustion of coals: correlation with fouling and slagging. Fuel Process Technol 42: 47–60

Sharp JH, Brindley GW, Achar NN (1966) Numerical data for some commonly used solid state reaction equations. J Am Ceram Soc 49: 376–382

Ten Brink HM, Eenkhoorn S, Weeda M (1996) The behaviour of coal mineral carbonates in a simulated coal flame. Fuel Process Technol 47: 233–243

Vidyasagar K, Gopalakrishnan J, Rao CNR (1984) A convenient route for synthesis of complex metal oxides employing solid-solution precursors. Inorg Chem 23: 1206–1210

Zakharov VY, Adonyi Z (1986) Thermal decomposition kinetics of siderite. Thermochim Acta 102: 101–107